

NUMERICAL AND EXPERIMENTAL ASSESSMENT OF VELOCITY WITH/WITHOUT MODEL INSIDE TAYLOR'S WIND TUNNEL TEST SECTION

ABDULKAREEM SH. MAHDI AL-OBAIDI*, LOW HENG YANG

School of Engineering, Taylor's University, Taylor's Lakeside Campus,
No. 1 Jalan Taylor's, 47500, Subang Jaya, Selangor DE, Malaysia
*Corresponding Author: abdulkareem.mahdi@taylors.edu.my

Abstract

A wind tunnel is a tool designed to determine the flow characteristics of air around a solid object that replicate the actual flow condition with designated similarities. It is important to study and analyse the flow conditions, such as velocity in the test section which is supposed to simulate the real flow conditions exactly. This research assesses the air flow velocity and velocity distribution in the test section of the subsonic suction-type wind tunnel available in Taylor's University with low Reynolds number. There are difference between the flow pattern in the test section and the ideal case simulated using numerical analysis model, in this case, computational fluid dynamics. The differences are compared to assess the accuracy and precision by determining the percentage error from the ideal flow conditions. For experimental analysis, the flow velocity of different data points in the Taylor's Wind tunnel were measured using the hot wire anemometer and the DAQ system so that the data can be tabulated and visualized in plotted graphs. As for numerical analysis, computational fluid dynamics (CFD) tool which is ANSYS FLUENT is used to model the flow in the test section using the SST $k-\omega$ turbulent model. The post processing unit of the software helped in the interpretation of the data collected in the simulation. The same was done with an aluminium NACA 0012 airfoil model inside Taylor's Wind tunnel test section. From this research, it is identified that the maximum is -6.96% and -3.16% when frequency is adjusted 15 Hz and 25 Hz to for case without model. For the case with model, the velocity varies at a maximum up to 2.94% and -3.16% when the frequency is 15 Hz and 25 Hz respectively. There is also a notable negative trend of velocity approaches the bottom wall may be due to leakage of air flow and elevated roughness.

Keywords: Low-speed wind tunnel, Test section, Flow velocity, CFD.

1. Introduction

A wind tunnel is a tool designed to measure the flow characteristics of air around the solid object that replicate the actual flow condition with designated similarities. Low-speed wind tunnels are wind tunnels that are capable with the operational flow speed of 134 m/s or Mach = 0.4 [1].

One of the first wind tunnels was invented around the 19th century [2]. In 1901, the Wright brothers used it to study the flow behavior around the different shapes to make their Wright Flyer [3]. Wind tunnels are designed based on different applications. There is one field that uses wind tunnels is the testing for atmospheric boundary conditions [4]. Ghani *et al.* analysed the performance of different critical components of a closed-loop full-scale climatic wind tunnel for road vehicle natural environment using CFD [5]. In aeronautics, wind tunnel nozzles are designed using CFD [6]. CFD was also used to interpret wind tunnel measurement result [7, 8].

Despite large improvement in computational power and capabilities so far, Wind tunnel has not been replaced by CFD but CFD had reached a point whereby the experimental and numerical results complement each other. Moonen *et al.* came up with a method of numerical model that simulates the steady-state conditions in a closed-loop wind tunnel using standard and realisable k- ϵ equation [9]. Their work provided a new benchmark to the accuracy of the wind tunnel model simulation. Gordon and Imbabi utilized CFD to model the flow inside critical sections of closed-loop wind tunnel [10]. The results obtained in this research demonstrated that proper classification of required improvement could improve the cost effectiveness and reduce the size of wind tunnels. Moonen *et al.* achieve six indices of similar characteristics to evaluate the flow quality in the test section in 3D in the CFD simulation [11].

In year 2010, another research is done by Guzella *et al.* [12] to numerically and experimentally assess the airflow inside a wooden-made low-speed wind. This test section has a length of 0.79 m and side and width of 0.2 m. Reynolds-Averaged Navier-Stokes (RANS) equations were solved numerically utilising ANSYS-CFX simulation software and the model used is the SST k- ω turbulence model. The velocities of the tunnel outlet were measured using a hotwire anemometer and a Pitot tube was compared with the numerical values of axial velocity. However, this research only focuses on the airflow exiting the tunnel test section which is not as accurate as the flow measure within the test section.

The wind tunnel that is used in this project is the subsonic open-type wind tunnel which has a suction fan to draw air. It has a better flow quality as compared to the blow-down wind tunnel. Taylor's wind tunnel contains a rectangular test sections measured 0.303 m by 0.303 m in cross section and 0.885 m in length. Test section speed can be adjusted by adjusting the fan speed from 3.33 m/s up to 38.35 m/s via a 3HP, 415 V/50 Hz, 0.63 m in diameter fan (KRUGER L06-RQ). The TUWT fan can generate subsonic flow with Mach number ranging from 0 to 0.1. Figure 1 depicts the Taylor's Wind Tunnel.

Lim [13] conducted experiment using Taylor's wind tunnel and compared the experimental results with published data by Abbott and Von Doenhoff [14]. Table

1 shows a comparison between the experimental and the published results. The table shows that the percentage error using Taylor’s wind tunnel is up to 49%.

To show a more comprehensive visualisation of sub-sonic wind tunnels, Table 2 is presented to compare the specifications of the existing facilities at different places around the world.



Fig. 1. Taylor’s wind tunnel.

Table 1. Percentage error in lift and drag coefficients obtained from wind tunnel tests at different Reynolds number [13, 14].

Angle of Attack	Re = 5×10 ⁴		Re = 1×10 ⁵		Re = 2×10 ⁵	
	C _L	C _D	C _L	C _D	C _L	C _D
-10	28.94	8.73	6.8	18.56	16.6	3.79
-5	26.03	30.79	16.97	48.79	11.7	27.52
0	2.72	6.51	10.0	28.59	7.3	3.9
5	5.62	27.4	1.16	37.66	15.3	19.79
10	9.8	13.01	14.84	10.0	25.2	17.48

Table 2. Specifications of existing subsonic wind tunnels.

	UNNE [15]	IPT WT [16]	University of Leeds [17]	Taylor's University [13]
Location	Chaco, Argentina	SaoPaulo, Brazil	Leeds, United Kingdom	Selangor, Malaysia
Circuit type	Opened-loop	Opened-loop	Closed-loop	Opened-loop
Application	Structural Engineering	Calibration	Civil Engineering	Calibration
Test section (m)	2.4 × 1.8	0.5 × 0.5	0.5 × 0.5	0.303 × 0.303
Air Velocity (m/s)	-	2.5 - 20	42036	3.3 - 38.4

Achieving accurate measurement of aerodynamic characteristics in the wind tunnel is challenging. It is subject to many factors, for instant the flow conditions in the test section. One important condition is to ensure that the flow velocity inside the test section is similar to the velocity of the prototype in real situation.

The current research addresses the challenge by numerical and experimental study and analysis of the flow velocity and the velocity distributions with or

without a model inside the test section of Taylor's wind tunnel. It aims to achieve uniformity of mean air velocity so that it can contribute directly to the accuracy of the tests in future.

2. Methodology

The research design of this project involves numerical and experimental approach. This research will compare the experimental data with the numerical result of the flow velocity in with and without a model inside the test section. The numerical approach will take advantage of the ANSYS FLUENT software available to generate the geometry, discretize the domain and solve the cases in ideal manner. On the other hand, for the experimental approach, the flow velocity is measured from 25 data point distributes across the test section by using a hotwire anemometer. The experimental data will then be compared with the numerical results to identify the error percentage in terms of velocity and velocity distribution.

2.1. Numerical method

In this paper the numerical approach used is Computational Fluid Dynamics (CFD) which is useful in performing engineering problem solving especially in flow studies. CFD provides the researcher the understanding of engineering designs and give a rough overview on the efficiency of the newly developed systems. ANSYS FLUENT is used in this research [18].

Here, only uses two governing equations which are used the conservation of momentum and conservation of mass [1]:

$$\frac{\partial \rho}{\partial t} + \vec{\nabla} \cdot (\rho U) = 0 \quad (1)$$

$$\frac{\partial(\rho U)}{\partial t} + \vec{\nabla} \cdot (\rho U \times U) = -\vec{\nabla} p' + \vec{\nabla} \cdot (\mu_{eff}(\vec{\nabla} U + (\vec{\nabla} U)^T)) + B \quad (2)$$

where U is mean velocity vector, ρ is fluid density, μ_{eff} represents effective viscosity contributing to turbulence, p' stands for modified pressure. The equation for μ_{eff} and p' are also given in as Eqs. (3) and (4) respectively.

$$\mu_{eff} = \mu + \mu_t \quad (3)$$

$$p' = p + \frac{2}{3}\rho k \quad (4)$$

Equation for μ_t can be describe as

$$\mu_t = C_\mu \rho \frac{k^2}{\varepsilon} \quad (5)$$

where μ is molecular viscosity, k represents turbulent kinetic energy, ε is the turbulent dissipation rate and C_μ stands for the model constant. The model constant is preset by ANSYS FLUENT beforehand.

Since wind tunnel is an enclosed channel, it is considered as an internal flow. The common model used to solve internal flows is the standard $k-\varepsilon$ turbulence model. However, this model does not produced accurate results when it comes to capturing the boundary layer effect thus it is not suitable for this simulation. Realizable $k-\varepsilon$ turbulence model an improved version of the $k-\varepsilon$ turbulence model. On the other hand, despite its better accuracy in solving the boundary

layer effect, it uses the enhance wall treatment as default which will not allow the input of wall roughness later in the research.

There is another model that is suitable for aerodynamic which is the realizable $k-\omega$ turbulent model. It has the best accuracy when it comes to capturing the boundary layer but the SST $k-\omega$ turbulence model is final choice as it combines the benefit of both the $k-\omega$ turbulence and the $k-\epsilon$ turbulence model. This two-equations model are very versatile and robust.

For geometry, the test section which is modelled has dimension based on the position at which the velocity is measurable using the hotwire anemometer in the experiment. To reduce the processing time, only half of the geometry is modelled. With the center of the test section set as origin, the test section is modeled in FLUENT as shown in Fig. 2. The middle plane is set as symmetry. The working domain is set to be fluid. Figure 3 shows the Mesh results for test section without model. Figures 4 and 5 show the geometric model and the mesh results of test section with model.

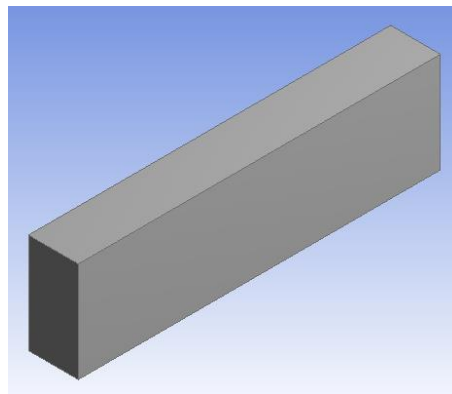
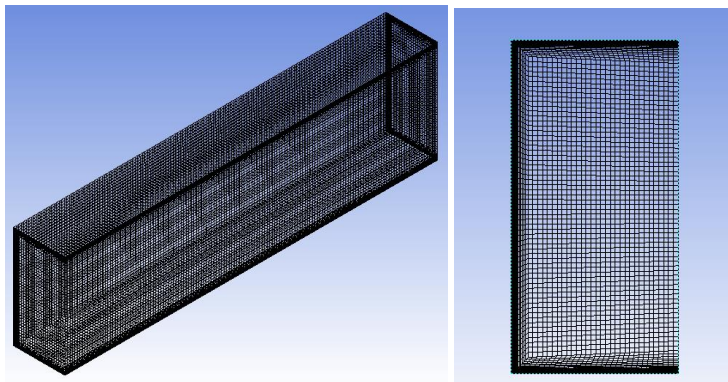


Fig. 2. Geometric model of test section without model.



(a) Isometric view

(b)Front View

Fig. 3. Mesh results for test section without model.

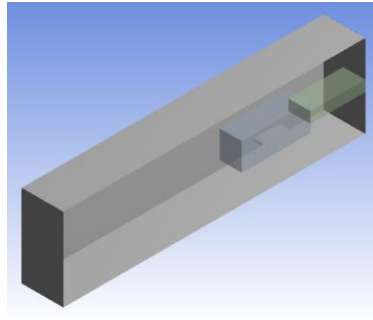
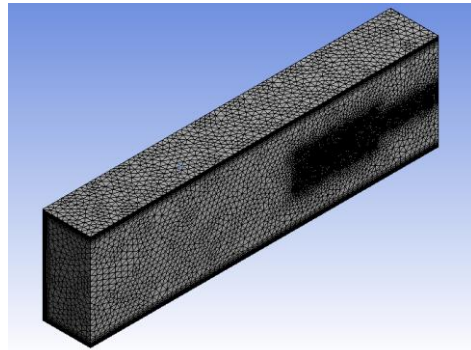
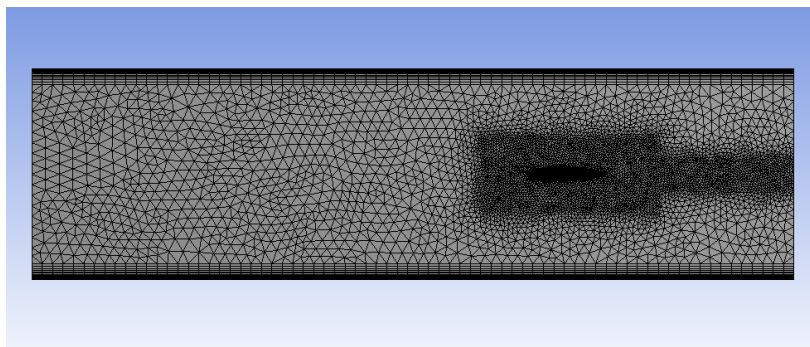


Fig. 4. Geometric model of test section with model.



(a) Isometric view



(b) Side View

Fig. 5. Mesh results for test section with model.

Different mesh types are used in this numerical simulation to acclimatize to specific conditions. Abbreviations are given to these different mesh types for the ease of reference as shown in Table A1. The details of input for mesh can also be found in Appendix A.

Boundary conditions that will be set include the inlet and outlet of the test section other than the wall of test section. To acquire the inlet velocity, the initial input is obtained from the calibration graph shown in Fig. 6. From this graph, it

can be seen that the calibration done recently has a slight difference compared to the data collected back in 2009 [19]. To achieve the more accurate input for the numerical simulation, the gradient, m of the straight lines are calculated in average and the offset, c is ignored. With the averaged gradient, the velocity for 15 Hz and 25 Hz are found to be 9.801 m/s and 16.335 m/s respectively.

However, all the velocities from this graph are obtained from the exact center of the test section with the coordinates of (0, 0, 0). These values are not accurate when it is used as the velocity of the inlet because this is the not the inlet velocity. To determine the inlet velocity for the simulation, estimation and trial an error is done until the velocity at the center of the test section is 9.801m/s and 16.335 m/s for 15 Hz and 25 Hz respectively. The results are shown in Table 3. From this table, the numerical inlet velocity is determined to be 9.862 m/s and 16.201 m/s for 15 Hz and 25 Hz respectively.

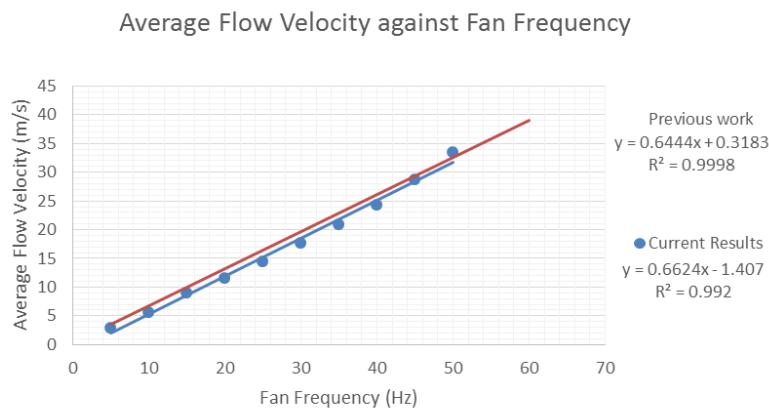


Fig. 6. Calibration graph of test section [19].

Table 3. Numerical velocity test across empty test section.

Fan Frequency (Hz)	Numerical inlet velocity (m/s)	Velocity at centre of test section (m/s)
15 Hz	9.801	9.922
	9.714	9.833
	9.682	9.801
25 Hz	16.335	16.468
	16.270	16.405
	16.201	16.335

As mentioned by ANSYS [20], when Mach numbers is equal to 1.0 or less, the effect of the compressibility may be neglected other that the deviation of the gas density against pressure is negligible. Therefore, the density is set at a constant of 1.225 kg/m³.

For the walls, it is impractical not to consider non-slip condition as it will affect the flow velocity at a relatively significant manner. Therefore, the assumption of non-slip condition is made. This shows that the friction along the wall is the highest resulting in the airflow velocity at the wall has zero value [21].

In the simulation, this means that the first layer of the mesh that have one of its sides connected to the solid wall will have zero velocity.

Since the wall of test section were made up of Plexi-glass, it is defined to have a roughness of 0.0000015 m roughness height. Moreover, for the case with CNC-machined aluminum model of NACA0012 airfoil inside, the wall of the model is set to have a roughness height of 0.00000984 m [22]. The walls of all test section and the surface of the airfoil model is assume to have an even surface with 0.5 roughness constant.

As for the outlet, the relative static pressure is assumed to be 0 Pa and the turbulent intensity is 5% which is originally set by FLUENT when initiated. Isothermal condition is assumed in this flow conditions. The simulation type is 3D pressure based for the solution method. The simulation is also considered to be a steady state flow which is independent of time. The pressure-velocity coupling scheme will be tested to identify the solver that requires the less time to achieve convergence in the results.

From Table 4, it can be seen that the SIMPLE scheme requires the least time for the solution to converge which is only 10 minutes and 23 seconds. Hence, it is chosen to compute the all the simulations results. The skewness correction is set to be 0. The spatial discretisation include the gradient of Least Square Cell Based. The Pressure, Momentum, Second Order while the Turbulent Kinetic Energy and Turbulent Dissipation rate is set to be First Order.

Table 4. Time taken for different solvers to solve WMAB 3.

Case	Solver	Time Taken (min: sec)
WMAB 3	SIMPLE	10:23
	SIMPLEC	14:30
	Coupled	10:43

2.2. Experimental method

The experimental equipment used is the Taylor's Wind Tunnel which has a contraction ratio of 3:4:1. The achievable air velocity by this low speed wind tunnel is from 3.33 m/s up to 38.35 m/s. The velocity can be controlled by adjusting the fan frequency with a recommended range of 10 Hz to 50 Hz. It is operated using a 3 HP, 415 V/50 Hz motor and 0.63 m of fan diameter. The square cross section of the test section is measured 0.303 m at the sides and it has a total length of 0.885 m. However, in this research, the inlet and outlet of the test section are considered to be located 0.35 m away from the center datum of the test section in the longitudinal direction. This is because there are holes drilled on the plexi-glass and the farthest holes are there. These holes are drilled so that the data for velocity can be collected when the hotwire anemometer is inserted into them.

For data collection, a hotwire anemometer with HVACR Datalogger which measures real time data will be used to obtain the flow velocity Holes had been made through the bottom of the test section wall for the hotwire to position through. The flow distribution had been measure by collecting set of data of flow velocity in different data points located at position distributed across the test section. The test section is separated by 5 sections which result in 5 plane

including the inlet and outlet of the test section. As the minimum data points established by ISO 3966:1977 to characterized the flow profile is 25, 25 data points is set on each planes from $x = -0.35$ to $x = +0.35$. As shown in Fig. 7, the x planes across the test section where the data points are collected with the hotwire positioned at coordinate (0, 0). Figure 8 shows the data points acquired from the cross section of the wind tunnel.

The data of velocity profile is collected initially without a model in the test section and later with a NACA0012 placed in at the coordinate (0, 0). The NACA0012 model is machined from a single block of aluminum which has a span of 0.068 m and a chord length of 0.10 m.

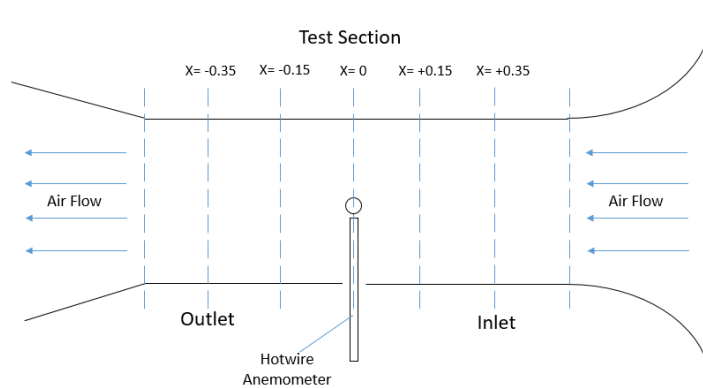


Fig. 7. Experimental setup.

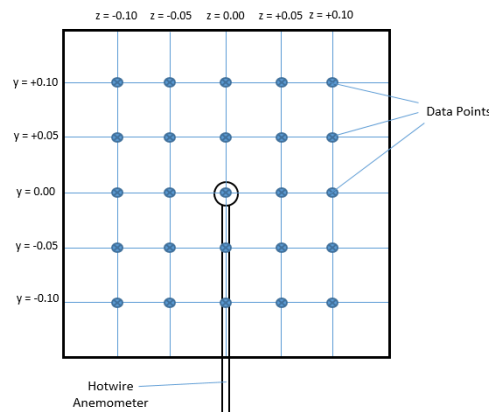


Fig. 8. Data points acquired from the cross section of the wind tunnel.

For the empty test section, velocity readings are collected from a total of 125 data points. Then, for the test section with NACA0012 model, the total number of data points that is needed to have velocity reading collected is 122 points. This is because the point located at the origin of the test section is occupied by the model while the 2 other points are occupied by the structure supporting the model. For each data points, only 3 readings of velocity are taken over a period of 10 seconds to reduce the random error.

3. Results and Discussion

Mesh analysis is done and the suitable mesh which is MWAB 3 and EM 3. Further details about mesh analysis can be found in Appendix. The final numerical results are taken from the mesh EM 3 and WMAB 3. These results are then used as a benchmark of the ideal flow in the test section when there are no external forces subjected to it. The results obtained from the experiment are compared to these data and the difference between the results are analysed.

Figures 9 and 10 illustrate the comparison of the experimental data of velocity obtained using the hotwire anemometer with the numerical results of the average velocity profile. Overall, it shows that there is a well agreement between the numerical result and the experimental data for both 15 Hz and 25 Hz of fan frequency. However, there are still some slight variations. For the case without model, the experimental data shows an increasing trend when y approaches the top wall. Flow velocity also decreases as y approaches the bottom wall.

In general, the correlation is considered to be fairly good. From Table 4.3, the experimental data only varies from the numerical results by a maximum of 6.96% and 3.16% at $y/H = -0.33$ for case without model when frequency is adjusted to 15 Hz and 25 Hz. For the case with model, the velocity varies at a maximum 2.94% at $y/H = 0.00$ and -3.16% at $y/H = -0.33$ when the frequency is 15 Hz and 25 Hz respectively.

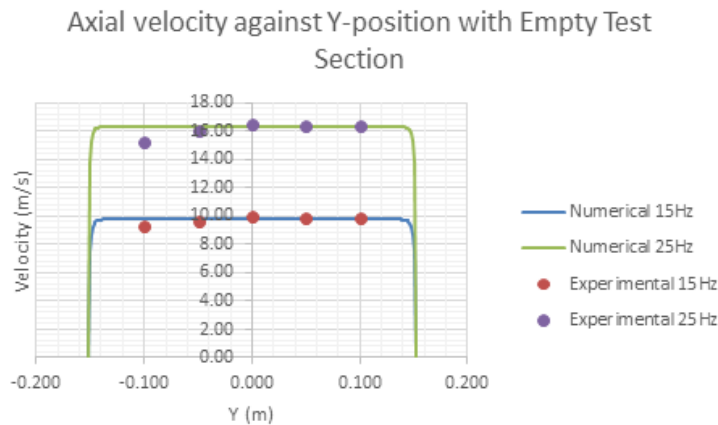


Fig. 9. Comparison of experimental and numerical results for empty test section.

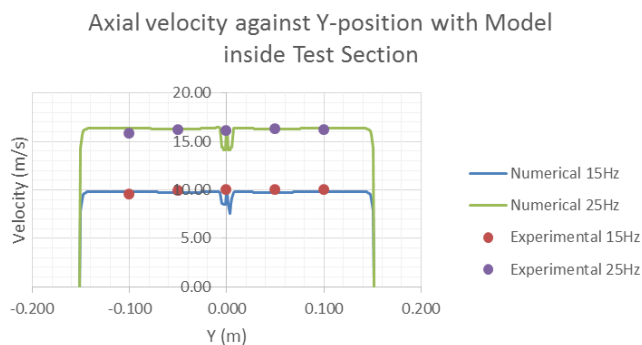


Fig. 10. Comparison of experimental and numerical results for test section with model.

Table 5. Percentage error of the velocity across the vertical position of test section.

y/H	Empty Test Section		Test Section With Model	
	15 Hz	25 Hz	15 Hz	25 Hz
	(9.801 m/s)	(16.335 m/s)	(9.801 m/s)	(16.335 m/s)
+0.33	0.30	0.43	2.10	-0.86
+0.17	0.97	0.01	2.89	-0.32
0.00	1.81	1.11	2.94	-0.32
-0.17	-2.14	-1.82	1.30	-0.43
-0.33	-4.99	-6.96	-2.30	-3.16

As seen from Table 5 and Figs. 9 and 10e, regardless of the existence of a model inside the test section, there is a negative trend of velocity towards the bottom of the test section wind based on the experimental data. This means as the position of the tunnel approaches the bottom wall of the wind tunnel; the measurement of velocity will be lower also.

The negative trend of the results when vertical position approaches the bottom wall of the wind tunnel may be caused by few possible reasons. One of the reasons that might cause this error is the outflow of air through the hole where the hotwire anemometer is placed through. Despite the effort to seal the drilled holes on the bottom wall with cellophane tape to reduce the outflow of air, it is very likely that it is not air tight enough. Other than that, the surface of the bottom test section wall also has elevated roughness as the repeated used of cellophane tapes to cover the drilled holes leave residues on it.

Another phenomena that may cause the errors in this research is the rapid fluctuation of the velocity reading from the datalogger that obtains the data from the hotwire anemometer. This fluctuation is cause by the turbulence in the flow. Therefore, it is better to collect the experimental data with more number of readings to in the future when the time constrain is less. Another source of error may be due to the insufficient data points for reading to be collected to achieve a mean results whereby random errors are negligible

4. Conclusions and Future work

In a nut shell, this research shows a comprehensive and clear comparison between the numerical and experimental correlations of velocity profile in the test section of Taylor's opened-loop suction type low-speed wind tunnel. Detail measurements done using hotwire anemometer and HVAC Datalogger were used to examine the flow velocity profile along center plane of the test section. SST $k-\omega$ turbulence model was used to compute the numerical results and were compared with the experimental data. Mesh independence was ensured for accurate results. The amount of variation of experimental data from the numerical result is computed to illustrate the accuracy of the wind tunnel when it is put into practical operation. In general, the correlation is considered to be fairly good. Experimental data only varies from the numerical results by a maximum of 6.96% and 3.16% for case without model when frequency is adjusted to 15 Hz and 25 Hz. For the case with model, the velocity varies at a maximum up to 2.94% and -3.16% when the frequency is 15 Hz and 25 Hz respectively. The negative trend is evident when the vertical position approaches the bottom wall. It is very likely to be cause by the leakage of air flow and elevated roughness.

Further study should be done on the boundary layer by measure velocity near the wall of test section in the experimental part since the results for the numerical simulation includes the boundary layer. The effect of the orientation of model towards the velocity profile may also by an interesting subject to be studied as well as the effect of different size of the model. This will help to identify the best orientation and size needed to achieve the most accurate results.

The supporting structure for the model may also be taken into consideration in the numerical simulation in the future to achieve more accurate results. This is because the supporting structure will also alter the flow velocity within the wind tunnel.

Acknowledgment

The authors would like to thank Taylor's University which provided an opportunity to utilise Taylor's wind tunnel and the ANSYS FLUENT 15.0 available to complete this research.

References

1. Barlow, J.B.; William, H.R.; and Pope, A. (1999). *Low-speed wind tunnel testing (3rd ed.)*. John Wiley & Sons.
2. Nguyen, Q.Y. (2014). Designing, constructing, and testing a low-speed open-jet wind tunnel. *International Journal of Engineering Research and Applications*, 4(1), 243-246.
3. Technology, T.M.I. (2002). *Wind tunnel Wright brothers*.
4. Maurer, T.; Herrmann, L.; Gaiser, T.; Mounkaila, M.; and Stahr, K. (2006). A mobile wind tunnel for wind erosion field measurements. *Journal of Arid Environments*, 66(2), 257-271.
5. Abdul Ghani, S.A.A.; Aroussi, A.; and Rice, E. (2001). Simulation of road vehicle natural environment in a climatic wind tunnel. *Simulation Practice and Theory*, 8(6-7), 359-375.
6. Korte, J.J. (1992). Aerodynamic design of axisymmetrical hypersonic wind-tunnel nozzles using a least-squares parabolized Navier-Stokes procedure. *Journal of Spacecraft Rockets*, 29(6), 870-871.
7. Moreau, S.; Henner, M.; Iaccarino, G.; Wang, M. and Roger, M. (2003). Analysis of flow conditions in freejet experiments for studying airfoil self-noise. *AIAA Journal*, 41(10), 1895-1905.
8. Cockrell, C.E. (1994). Interpretation of waverider performance data using computational fluid dynamics. *Journal of Aircraft*, 31(5), 1095-1100.
9. Moonen, P.; Blocken, B.; Roels, S.; and Carmeliet, J. (2006). Numerical modeling of the flow conditions in a closed-circuit low-speed wind tunnel. *Journal of Wind Engineering and Industrial Aerodynamics*, 94(10), 699-723.
10. Gordon, R.; and Imbabi, M. (1998). CFD simulation and experimental validation of a new closed circuit wind/water tunnel design. *Journal of Fluids Engineering*, 120(2), 311-318.
11. Moonen, P.; Blocken, B.; and Carmeliat, J. (2007). Indicators for the evaluation of wind tunnel test section flow quality and application to a numerical closed-

circuit wind tunnel. *Journal of Wind Engineering and Industrial Aerodynamics*, 95(9-11), 1289-1314.

12. Guzella, M.S.; Manto, D.; Soares, C.B.; Maia, C.B.; Hanriot, S.M.; and Cabezas-Gómez, L. (2010). Airflow CFD modeling in the test section of a low-speed wind tunnel. *Journal of Advanced Research in Mechanical Engineering*, 1(4), 210-225.
13. Lim, W.K.; Al-Obaidi, A.S.M. (2013). *Taylor's wind tunnel manual*. Taylor's University Subang Jaya, Malaysia.
14. Abbott, I.H.; and Von Doenhoff, A.E. (1999). *Theory of wing sections: including summary of airfoil data*. Mineola: Dover Publications.
15. Wittwer, A.R.; and Moller, S.V. (2000). Characteristics of the low-speed wind tunnel of the UNNE. *Journal of Wind Engineering and Industrial Aerodynamics*, 84(3), 307-320.
16. Nader, G.; dos Santos, C.; Jabardo, P.J.S.; Cardoso, M.; Taira, N.M.; and Pereira, M.T. (2006). Characterization of low turbulence wind tunnel. *XVIII IMEKO World Congress*, Rio de Janeiro, Brazil, 17-22.
17. Calautit, J.K.; Chaudhry, H.; Hughes, B.R.; and Sim, L.F (2014). A validated design methodology for a closed loop subsonic wind tunnel. *Journal of Wind Engineering and Industrial Aerodynamics*, 125, 180-194.
18. Versteeg, H.K.; and Malalasekera, W. (1995). *An introduction to computational fluid dynamics. The finite volume method*. Longman Group Ltd.
19. Al-Obaidi, A.S.M.; Lee, C.S.; Tan, K.; Lee, H.I.; Singh, K.; and Foo, T. (2009), Velocity - frequency calibration curve. Taylor's College, Subang Jaya, Selangor.
20. ANSYS (2013), *ANSYS Fluent User's Guide*, Southpointe, Pennsylvania: ANSYS Inc.
21. Young, D.F.; Munson, B.T.; Okiishi, T.H.; and Huebsch, W.W. (2012), *Introduction to Fluid Mechanics*. John Wiley & Sons, Inc.
22. Dilworth, R.L. (1967). Aerospace metals- General data and usage factors. *Technical manual*. Engineering series for aircraft repair, US Army.

Appendix A

Numerical Method Details

Table A1. Abbreviations for different mesh types.

Abbreviations	Conditions	Cell Shape
EM	Empty, Multi-zone	Hexahedral
EANB	Empty, Automatic, No Body of Influence	Tetrahedral
EAB	Empty, Automatic, Body of Influence	Tetrahedral
WMAB	With model, Automatic, Body of Influence	Tetrahedral

Table A2. Input of mesh dependency test 15 Hz (9.801 m/s).

Case	Mesh sizing around model (m)	Mesh sizing across test section (m)	Face sizing around model (m)	First layer thickness (m)	
				Around model	along test section
EM 1	-	0.02	-	-	0.0002100
EM 2	-	0.015	-	-	0.0001400
EM 3	-	0.01	-	-	0.0000700

EM 4	-	0.0075	-	-	0.0000700
EANB	-	0.015	-	-	0.0000576
EAB	0.0035	0.015	-	-	0.0000576
WMAB 1	0.0056	0.024	0.0046	0.0001	0.0001250
WMAB 2	0.0042	0.018	0.0032	0.0000700	0.0001000
WMAB 3	0.0035	0.015	0.0019	0.0000390	0.0000576
WMAB 4	0.0029	0.012	0.0019	0.0000390	0.0000576

Table A3. Input of mesh dependency test with 25 Hz (16.335 m/s).

Case	Mesh sizing around model (m)	Mesh sizing across test section (m)	Face sizing around model (m)	First layer thickness (m)	
				Around model	along test section
EM 1	-	0.02	-	-	0.0001300
EM 2	-	0.015	-	-	0.0000700
EM 3	-	0.01	-	-	0.0000422
EM 4	-	0.0075	-	-	0.0000422
EANB	-	0.015	-	-	0.0000576
EAB	0.0035	0.015	-	-	0.0000354
WMAB 1	0.0056	0.024	0.0046	0.00008	0.0001200
WMAB 2	0.0042	0.018	0.0032	0.0000400	0.0000700
WMAB 3	0.0035	0.015	0.0019	0.0000200	0.0000354
WMAB 4	0.0029	0.012	0.0019	0.0000200	0.0000350

Table A4. Mesh dependency results for 15 Hz (9.801 m/s).

Case	Number of elements	Minimum orthogonal quality	Maximum skewness	y+		Time taken
				Around model	Along test section	
EM 1	65340	0.4946	0.6224	-	2.90	0:26
EM 2	84169	0.4557	0.5711	-	1.92	0:29
EM 3	193980	0.4620	0.5314	-	0.99	1:10
EM 4	407190	0.5693	0.5314	-	1.00	2:38
EANB	250697	0.1342	0.8918	-	1.00	1:42
EAB	982509	0.1463	0.8499	-	1.00	8:29
WMAB 1	420797	0.0167	0.9193	1.84	2.15	3:23
WMAB 2	693740	0.0217	0.8981	1.46	1.70	6:26
WMAB 3	1133714	0.0304	0.8796	1.00	1.00	10:23
WMAB 4	1742625	0.0304	0.8796	0.99	1.02	18:27

Table A5. Mesh dependency results for 25 Hz (16.335m/s).

Case	Number of elements	Minimum orthogonal quality	Maximum skewness	y+		Time taken
				Around model	Along test section	
EM 1	65340	0.4031	0.5649	-	2.93	0:27
EM 2	84169	0.3185	0.5314	-	1.60	0:34
EM 3	193980	0.3635	0.5181	-	1.01	1:18
EM 4	407190	0.4933	0.5181	-	1.02	2:34
EANB	264726	0.0935	0.8995	-	1.02	1:55
EAB	998343	0.0937	0.8993	-	1.02	10:56
WMAB 1	420601	0.0134	0.9402	2.44	3.24	5:34
WMAB 2	714608	0.0123	0.8863	1.50	1.94	7:18
WMAB 3	1164374	0.0158	0.8760	1.00	1.02	11:46
WMAB 4	1784123	0.0158	0.8760	1.00	1.04	19:29

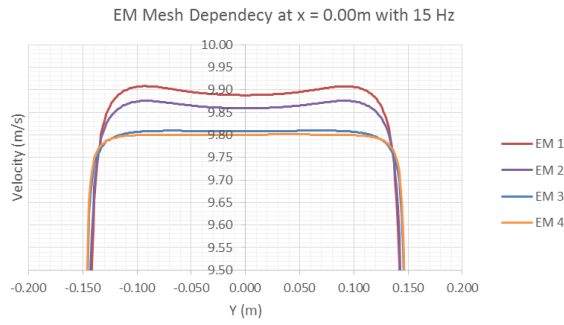


Fig. A1. Mesh dependency results for EM with 15 Hz (9.801 m/s).

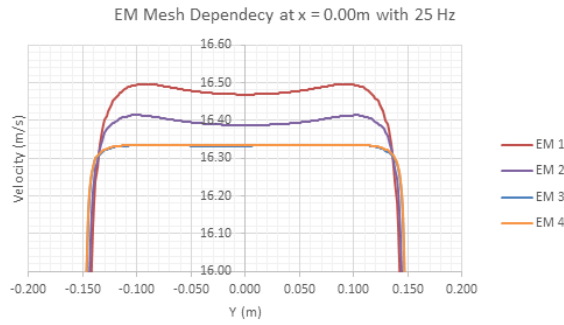


Fig. A2. Mesh dependency results for EM with 25 Hz.

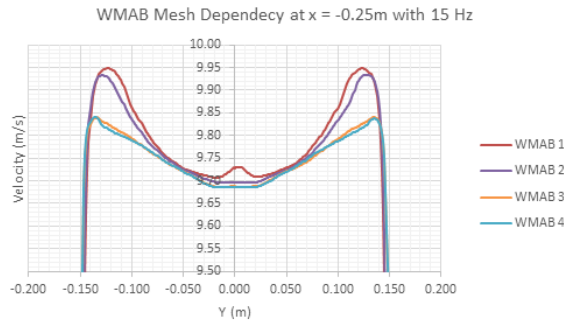


Fig. A3. Mesh dependency results for WMAB with 15 Hz (9.801 m/s).

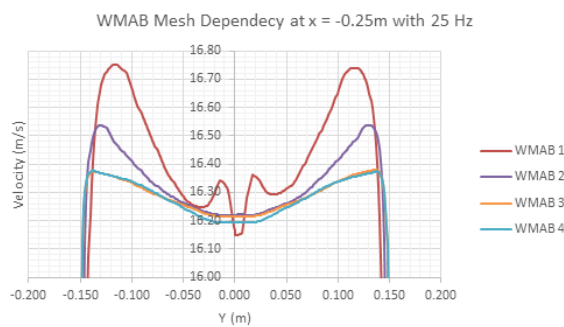


Fig. A4. Mesh dependency results for WMAB with 25 Hz (16.335 m/s).